IEEE Access
Multidisciplinary | Rapid Review | Open Access Journal

Received November 17, 2020, accepted November 21, 2020, date of publication November 25, 2020,
date of current version December 9, 2020.

Digital Object Identifier 10.1109/ACCESS.2020.3040430

Application of Kuramoto Model to Transmission Power Control in Wireless Body Area Networks

KIMCHHEANG CHHEA, DARA RON, AND JUNG-RYUN LEE, (Senior Member, IEEE)
School of Electrical and Electronics Engineering, Chung-Ang University, Seoul 06974, South Korea

Corresponding author: Jung-Ryun Lee (jrlee@cau.ac.kr)

This work was supported in part by the Ministry of Science and ICT (MSIT), South Korea, through the Information Technology Research Center (ITRC) Support Program, supervised by the Institute for Information and Communications Technology Planning and Evaluation (IITP), under Grant IITP-2020-2018-0-01799, and in part by the National Research Foundation of Korea (NRF) Grant funded by the Korean Government (MEST) under Grant NRF-2020R1A2C1010929.

ABSTRACT Wireless body area networks (WBANs) exhibits immense potential for application in ubiquitous healthcare systems. However, in dense environments where multiple WBANs are deployed such as hospitals, the performance of WBANs is deteriorated by inter-network interference. In this study, we apply Kuramoto model to the transmission power control of users in WBAN environments with the purpose of addressing the issue of inter-network interference, and thereby improving the Quality of Service (QoS) fairness in WBAN environment. For this purpose, we define the utility function which expresses the QoS of a user and synchronize this utility function value of each user for fair resource allocation. The synchronization of the utility function is obtained by Kuramoto model and coupling coefficient defined in Kuramoto model is dynamically adjusted for faster convergence. The range of convergence of the Kuramoto model is derived analytically. From the simulation results, we can verify that the performance of the proposed algorithm is better than those of the existing algorithms with regard to QoS fairness, power, and data rate. In addition, we show that the convergence speed of the proposed algorithm with adaptive coupling strength parameter outperforms the Kuramoto model with fixed coupling strength parameter.

INDEX TERMS Kuramoto model, quality of service (QoS), transmission power control, wireless body area networks (WBANs).

I. INTRODUCTION

With the rapid advancements in wireless communication technologies and sensor devices, wireless body area networks (WBANs) are becoming increasingly popular in ubiquitous healthcare [1]. Owing to the small size and life-long battery of the sensor node, WBAN gives users constant monitoring while allowing them to conduct their routine activities without interruption [2]. By offering real-time monitoring, WBAN can help in early detection and diagnosis of disease, which is cost and treatment-effective [3]. A WBAN system can consist of many sensor nodes and a coordinator node that are placed around or in the user's body. The sensors send information to the sink node, and the coordinator node relays the information to users. In WBAN system, there are typically three tiers of communication: intra, inter, and Beyond-WBAN communication. Intra-WBAN communication basically deals with the connection of the sensors that are placed approximately two meters around the body, while inter-WBAN communication additionally takes into account the coordinator that acts as access point for the sensor. The last tier is related to database that contains all of the patients' information [4]. Due to the growing applications of WBAN, the requirements of scalability, energy consumption, power usage, and resource allocation of the networks have also increased [5]. This poses challenges such as channel interference, power control, resource allocation, and security and privacy problems, which have garnered considerable research attention [6]–[8].

Transmission power control partakes a crucial role in wireless network, for it can affect the efficiency of resource utilization in a network. Due to the variation in channels' quality over time, the authors in [9] proposed a mechanism that predicts the received signal strength indicator (RSSI) by using gait cycle information in order to update the real-time transmission power level. Various studies have been conducted based on game theory to alleviate interference with coexisting WBAN. To reduce inter-WBAN interference, a non-cooperative power control game to control transmission power was proposed [10]. Each player is always trying

The associate editor coordinating the review of this manuscript and approving it for publication was Noor Zaman.

to find its own utility function to achieve maximum value. By adjusting the optimal transmission power, the players maximize their utilities through sink node using Nash equilibrium depending on the noise, channel's quality, signal-to-interference-plus-noise ratio (SINR), and initial transmission power of other players.

Recently, problems in wireless networks such as channel interference, power control, and resource allocation have been solved by using synchronization models. Synchronization is a process in which two or more disordered systems adapt an attribute of their motion to a mutual behavior according to other systems in their environment due to coupling or forcing [11]. The synchronization phenomenon of behavior in nature can be found in many live forms on Earth such as behaviors of fireflies flashing in group, flocking of birds, fish swimming in school, or pacemaker cells [12].

Among the many models, Kuramoto synchronization model is one of the mathematical model that gains popularity these days. Kuramoto model consists of independent oscillators that rotate at varying intrinsic frequencies coupled through the phase differences in sine function. As the coupling strength tends to a certain value in the critical region, the rotation speed of each oscillator achieves synchronization. Kuramoto model was originated in 1975 by Kuramoto Yoshiki [14]. Since then, many extensions and modifications of the model were documented in literature.

In this paper, we develop a transmission power control approach in WBAN environment to reduce inter-WBAN interference and satisfy the QoS of each user. The proposed algorithm is integrated with the Kuramoto model in order to synchronize the user's QoS. We also propose a coupling strength adjustment algorithm which varies coupling strength parameter value for faster convergence speed. The proposed algorithm shows stable convergence speed even the number of node increases, which validates the scalability of the proposed model. To sum up, we make three main contributions in this paper:

1) We apply the Kuramoto model to the power control in WBAN in order to mitigate interference and provide QoS fairness among users.
2) We propose coupling strength coefficient adjustment procedure to accelerate the convergence of the Kuramoto model.
3) We prove the convergence condition of the proposed algorithm.

This paper is organized as follows. In Section II, we explain the Kuramoto model with coupling strength coefficient adjustment which is one of the main contribution of this paper. In Section III, we describe the system model and the proposed transmission power control algorithm. In Section IV, we provide the proof regarding the convergence of the Kuramoto with coupling strength coefficient adjustment. In Section V, we evaluate the performance of the proposed algorithm. Finally, we conclude this paper in Section 6.

II. KURAMOTO MODEL WITH COUPLING STRENGTH COEFFICIENT ADJUSTMENT

Kuramoto model was originally developed as a tractable mean-field model of coupled biological oscillator, such as groups of chorusing crickets, fish swimming in school, and cardiac pacemaker cells [14]. In physics and biology, it has been used to study synchronization phenomena in populations of coupled oscillators [15]. Due to the distributed manner under which the Kuramoto model operates, it has been applied to in many fields of research [16]–[18]. For example, Moioli *et al.* applied Kuramoto model to investigate neural dynamics of a simulated robotic agent engaged in minimally cognitive tasks [19]. Authors in [18] studied the attractivity properties of the phase-locked equilibria set in nonlinear, heterogeneously delayed oscillator networks under fixed and switching topologies provided by Kuramoto dynamics.

In the Kuramoto model, suppose there are N oscillators, each characterized by a phase angle $\theta_i(t)$ at time t, and intrinsic frequency ω_i. The synchronization state of the oscillators can be achieved by the using the updating rule as the following equation:

$$\frac{d\theta_i}{dt} = \omega_i - \frac{K}{N}\sum_{j=1}^{N}\sin(\theta_j - \theta_i), \quad i = 1, 2, \ldots, N \tag{1}$$

where K is the coupling strength, which indicates the force that couples oscillators. An earlier study [22] has shown that when the coupling strength increases to a certain threshold, the collective behavior of the group of oscillators emerges. It is noted that the original Kuramoto model assumed that *constant* coupling strength coefficient for updating the phase. In this work, we take a note on the fact that when the initial phase values of oscillator are close to the convergent phase being synchronized, a large coupling strength is not needed, but when the initial values of oscillators are far away from those being synchronized, a large coupling strength might be suitable. Therefore, by varying the coupling strength according to the difference of initial values, the system can reach synchronization state faster than when using the constant coupling strength coefficient.

Here, we explain the proposed discrete-time Kuramoto model with coupling strength coefficient adjustment, which is to be applied to the power control in WBAN application. By considering that the frequencies of all the oscillators are identical, i.e., when $\omega_i = \omega$, we consider the discrete-time Kuramoto model, which is given by

$$\theta_i(t+1) = \theta_i(t) + \sum_{j=1}^{N} K_{ij}(t)\sin(\theta_j(t) - \theta_i(t)), \tag{2}$$

where K_{ij} is the coupling strength coefficient between oscillators i and j. In our work, K_{ij} is set to be updated according to the following equation;

$$K_{ij}(t+1) = \alpha K_{ij}(t) + \beta|\sin(\theta_j(t) - \theta_i(t))|, \tag{3}$$

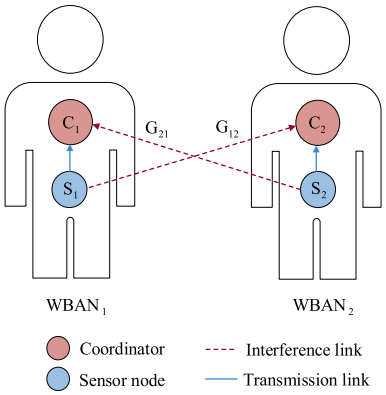

FIGURE 1. Inter-network interference model.

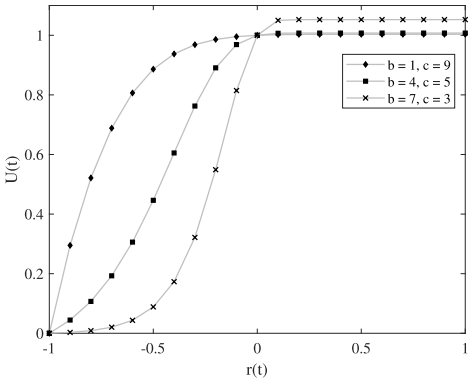

FIGURE 2. Utility function.

where α and β are non-negative constants that are proportional to learning enhancement rate and friction, respectively.

III. SYSTEM MODEL

As described in Section I, WBANs system consists of many bodies, and each body can consist of one coordinator, and up to ten sensor nodes in one network [20]. If transmission power range of several nodes overlap, they can interfere with each other as shown in Fig. 1. Based on the IEEE 802.15.6 standard, by assuming free intra-network interference, sensor nodes that are connected to the same coordinator can avoid interfering with each other through using multiple access techniques such as time division [21].

So, we assume that each WBAN $WBAN_i$ comprises of only one coordinator C_i and sensor node(s) S_i for simplicity, where S_i has different QoS requirement. Let G_{ii} and G_{ji} be the channel gain between sensor node S_i and coordinator C_i, and the channel gain between S_j and C_i, respectively. S_j is the sensor node that is within the range of C_i but is not connected to C_i. The signal-to-noise-interference (SINR) of S_i, γ_i at time t is expressed as follows:

$$\gamma_i(t) = \frac{p_i(t)G_{ii}}{\sum_{j=1,j\neq i}^{M} p_j(t)G_{ji} + N_0}, \tag{4}$$

where $i = \{1, 2, \ldots, N\}$, and $j = \{1, 2, \ldots, M\}$ are the set of WBAN, and sensor node(s) in a WBAN respectively, $p_i(t)$ and $p_j(t)$ are the transmit power of S_i in $WBAN_i$ and the neighboring S_j in $WBAN_j$, respectively, and N_0 is the noise. According to Shannon's capacity formula, the data rate $D_i(t)$ of the ith sensor node at time t is defined as follows:

$$D_i(t) = B\log_2(1 + \gamma_i(t)), \tag{5}$$

where B is the bandwidth of the channel.

A. PROPOSED ALGORITHM

Since each node can achieve a global purpose by processing and obtaining information from other nodes, the Kuramoto model described as in (2) is appropriate for use in distributed resource allocation. Here, we propose a power control algorithm based on Kuramoto model for WBAN environment. In the proposed algorithm, the utility function is used for defining QoS of each user, and the transmission power is adjusted to synchronize the value of utility. We use the utility function to express the QoS of each user according to data rate. The utility functions employed in previous study usually had sigmoidal or logarithmic form [23], [24]. According to Suzuki et al [23], the shapes of the utility functions are applied based on the type, and features of the applications in use. The utility value $U_i(t)$ of the sensor node S_i in $WBAN_i$ at time t can be written as follows:

$$U_i(t) = U_{max} - \frac{e^{-ce^{b.r(t)}}}{e^{-ce^{-b}} - e^{-c}} \tag{6}$$

where b and c are the parameters for controlling the shape of the utility function ($b > 0, c > 0$),

$$r(t) = \frac{D_i(t) - D_i^{Req}}{D_i^{Req}}, \quad -1 \leq r(t) < \infty, \tag{7}$$

and D_i^{Req} is the required data rate of sensor node S_i. The shape of the utility function can be changed according to the controlling parameters, b and c. For example, when $b = 1, c = 9$, and $b = 7, c = 3$, the utility exhibits the logarithmic and sigmoidal shapes, respectively, as can been seen in Fig. 2. The term, $U_{max} = 1 + e^{-c}/(e^{-ce^{-b}-e^{-c}})$, represents the maximum achievable value of utility. In this paper, D_i^{Req} is a constant and predetermined value for each user, and does not change over time. The value of $r(t)$ is greater than or equal to -1, and the lowest possible value of $D_i(t)$ is zero. If $D_i(t)$ is zero, the values of $r(t)$ is -1; hence, $U_i(t)$ is zero. If the values of $D_i(t)$ is the same as $D_i^{Req}(t)$, the value of $r(t)$ is zero; hence, the value of $U_i(t)$ is one. The transmission power required to convert From $D_i(t)$ to $D_i^{Req}(t)$ can be obtained from (4) and (5) as follows:

$$\begin{aligned} D_i^{Req}(t) &= B\log_2\left(1 + \gamma_i^{Req}(t)\right) \\ &= B\log_2\left(1 + \frac{p_i^{Req}(t)G_{ii}}{\sum_{k=1,j\neq i}^{N} p_j(t)G_{ji} + N_0}\right) \\ &= B\log_2\left(1 + p_i^{Req}(t) \times \frac{\gamma_i^{Req}(t)}{p_i(t)}\right) \end{aligned} \tag{8}$$

where $\gamma_i^{Req}(t)$ and $p_i^{Req}(t)$ are the SINR required for the coordinator C_i to attain the required data rate R_i^{Req} considering the channel gain and interference from neighbouring WBANs at

Algorithm 1 TPC Based on Kuramoto Model Algorithm

Parameters: $p_i(t)$, $\gamma_i(t)$, D_i^{Req}, $U_i(t)$, ϵ;
1: **for** $i \leftarrow 1, n$ **do**
2: **while** $|U_i(t+1) - U_i(t)| \geq \epsilon$ **do**
3: S_i transmits data packet to C_i;
4: S_i computes $\gamma_i(t)$ and $D_i(t)$ as in (4) and (5);
5: C_i calculates $U_i(t)$ as in (6);
6: **if** $U_i(t) > 1$ **then**
7: C_i calculates $p_i(t)$ according to (9),
8: $p_i(t) = p_i^{Req}(t)$;
9: **else**
10: $p_i(t) = p_i(t)$;
11: **end if**
12: C_i transmits its U_i information to all nodes;
13: C_i calculates the next utility $U_i(t+1)$ as in (10);
14: **if** $|U_i(t+1) - U_i(t)| \geq \epsilon$ **then**
15: C_i calculates $p_i(t+1)$ according to (11);
16: $p_i(t) = p_i(t+1)$
17: **else**
18: $p_i(t) = p_i(t)$;
19: **end if**
20: **end while**
21: **end for**
22: **return** p_i^*, D_i^*, U_i^* after $|U_i(t+1) - U_i(t)| < \epsilon$ for all i

time t, and the required power for obtaining the required data rate, respectively. From (8), we can compute $p_i^{Req}(t)$ given by

$$p_i^{Req}(t) = \max\left[p_{min}, \min\left[p_{max}, \left(2^{\frac{D_i^{Req}}{B}} - 1\right).\frac{p_i(t)}{\gamma_i(t)}\right]\right], \quad (9)$$

where p_{min} and p_{max} are the predetermined minimum and maximum transmission power, respectively. The coordinator C_i computes the next target utility value by using the Kuramoto model as below:

$$U_i(t+1) = U_i(t) + \sum_{j=1}^{N} K_{ij}(t)\sin(U_j(t) - U_i(t)) \quad (10)$$

where N is the number of sensor nodes. C_i can obtain the next target data rate by adjusting transmission power at the time $t+1$ based on the calculated utility value. $p_i(t+1)$ can be acquired based on (5) and (6), and can be expressed as follows:

$$p_i(t+1) = \max\left[p_{min}, \min\left[p_{max}, \frac{p_i(t).(2^{\frac{\rho}{B}} - 1)}{\gamma_i(t)}\right]\right] \quad (11)$$

where $\rho = D_i^{Req}\left(1 + \frac{1}{b}\ln\left(-\frac{1}{c}\left(\ln\left(\delta\left(U_{max} - U_i(t)\right)\right)\right)\right)\right)$, and $\delta = e^{-ce^{-b}} - e^{-c}$.

In the proposed algorithm (Algorithm 1), the initial value of transmit power are uniformly random between p_{min} and p_{max}. The required data rate is predetermined fixed value (see Table 1). The outputs of the algorithm are the adjusted transmit power p_i^*, data rate D_i^*, and utility U_i^*. The outputs of the algorithm can be determined according to the threshold, ϵ.

TABLE 1. Application of sensors used in simulation.

Type	Application	Data rate
1	ECG	0.192 Mbps
2	Cochlear implant	0.98 Mbps
3	EMG	1.536 Mbps
4	Capsule Endoscope	2.5 Mbps

When the difference between $U_i(t+1)$ and $U_i(t)$ is smaller than ϵ, then it means that $U_i(t+1)$ is the adjusted utility U_i^*. Hence, the adjusted transmit power and data rate are also determined when the utility is adjusted.

Step 1 is the beginning of the main loop. The loop runs repetitively for each node i until the criterion is met, that is until all nodes achieve convergence with the condition $|U_i(t+1) - U_i(t)| < \epsilon$. In step 3, S_i sends packets to C_i for processing. In the next step (step 4), S_i computes the SINR at time t $\gamma_i(t)$ and $D_i(t)$ according to the received packets. Subsequently, in step 5 C_i calculates the utility value for S_i at time t, which is $U_i(t)$. Then in step 6, $U_i(t)$ is determined using equation (6). In step 7, the case that the utility value $U_i(t)$ is greater than one means that the current data rate is greater than the required value, $D_i(t) > D_i^{Req}$. Hence, in step 8 the coordinator C_i decreases the transmission power of S_i such that the current data rate $D_i(t)$ becomes equal to the required data rate D_i^{Req}. By using the information of the SINR at time t, the required power for converting $D_i(t)$ to D_i^{Req} can be obtained from (9). However, if the utility value $U_i(t)$ smaller than 1, the transmit power $p_i(t)$ of sensor S_i stays the same. In the next step (step 12), C_i broadcasts its information to all the users. Next, in step 13, C_i calculates the next target utility $U_i(t+1)$ by using Kuramoto model. In step 14, the updated utility is compared with the utility value at previous time to see if the difference is larger or equal to a predefined threshold ϵ. Then, in step 15, C_i calculates the next step transmission power at time $t+1$, $p_i(t+1)$, which is updated according to equation (11). In step 18, if the difference of $U_i(t+1)$ and $U_i(t)$ is smaller than ϵ, the transmission power remains the same. The last step (step 22) is the end of the iteration loop.

Overall, there are eight main stages in the proposed algorithm as can be seen in Fig. 3. To begin with, the initial value $(p_i(t), \gamma_i(t), D_i^{Req}, U_i(t), \epsilon;)$ is set in the first stage. In stage two, the transmission of packets is in process between coordinator C_i and sensor node S_i. Next, the coordinator C_i compares the utility value $U_i(t)$ whether it is greater than 1; if so, the transmit power $p_i(t+1)$ is adjusted to achieve $U_i(t) = 1$; if not, the algorithm skips stage four and proceed to stage five. In stage five, the coordinator C_i shares the utility information of itself to neighboring node. In the following stage, C_i updates the transmit power $p_i(t+1)$ so that its utility value at time $t+1$ $U_i(t+1)$ is tuned according (10). Next, the stages two to six are repeated until the convergence criteria (the difference between the utility values at time t and $t+1$ becomes less than threshold ϵ) is satisfied. If the condition is met, the algorithm returns outputs, if not, the coordinator C_i readjusts the transmit power and returns to stage two until the condition in stage seven is met.

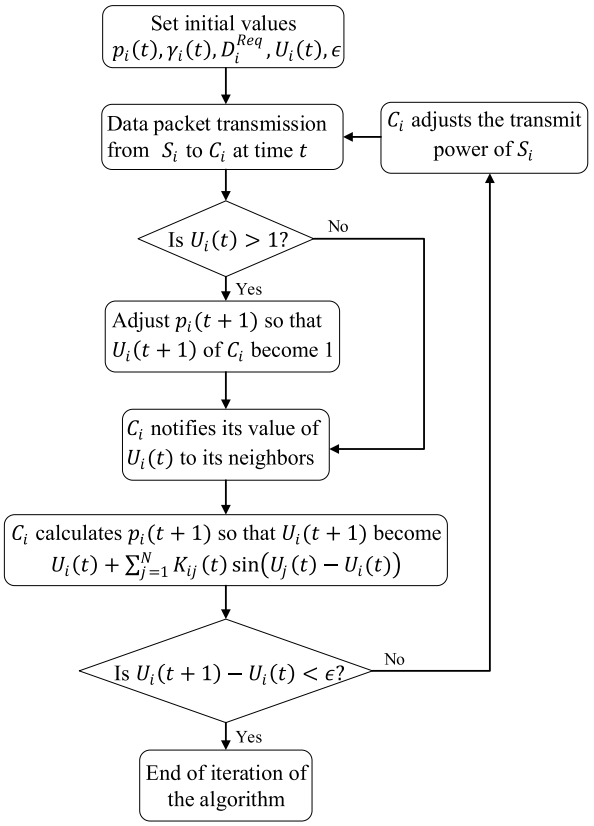

FIGURE 3. Flow chart of the proposed algorithm.

IV. ANALYSIS ON CONVERGENCE

In this section, we derive the condition for the convergence of the Kuramoto model with coupling strength coefficient adjustment.

Theorem 1: Suppose there are N objects in the network that updates their phases according to (2). When K_{kj} is initialized uniformly random in the interval $[0, \frac{\pi}{2N}]$, the phase oscillator $\theta_i(t) \in [0, \pi]$, $\alpha \in [-1, 1]$, and $\beta = \frac{\pi(1-\alpha)}{4N}$, then synchronization is achieved.

Proof: To prove Theorem 1, we construct a Lyapunov function. Let $\nabla(t)$ be the differential of Lyapunov at time t, $V(t)$ be the Lyapunov candidate at time t, and $V(t+1)$ be the updated function of the Lyapunov candidate at time $t+1$. It is known that $0 \leq V(t) \leq 1$ for $\forall t \in \mathbb{R}^+$. It is noted that $V(t) = 1$ for the synchronized states, and $V(t) = 0$ for the de-synchronization states. When $\nabla(t)$ approaches zero at time t, the system reaches convergence. We will prove that the Lyapunov differential at time t is greater or equal to zero, which can be described as follows:

$$\nabla(t) = V(t+1) - V(t) \geq 0. \tag{12}$$

In the following, we will prove that when Lyapunov differential is greater than or equal to zero when $\alpha \in [-1, 1]$. First, the phase centroid is obtained by

$$R(t) = \frac{1}{N} \sum_{k=1}^{N} \begin{vmatrix} \cos\theta_k(t) \\ \sin\theta_k(t) \end{vmatrix}. \tag{13}$$

We defined $V(t)$ as the square of the magnitude of the phase centroid, which is given by

$$V(t) = \|R(t)\|^2 = \left\| \frac{1}{N} \sum_{k=1}^{N} \begin{vmatrix} \cos\theta_k(t) \\ \sin\theta_k(t) \end{vmatrix} \right\|^2. \tag{14}$$

Then we have

$$\begin{aligned} \nabla(t) &= \frac{1}{N}\left(\left(\sum_{k=1}^{N} \sin\theta_k(t)\right)^2 + \left(\sum_{k=1}^{N} \cos\theta_k(t)\right)^2\right) \\ &= \frac{1}{N^2}\left(N + 2\sum_{k=1}^{N}\sum_{j=k+1}^{N} N\cos\left(\theta_k(t) - \theta_j(t)\right)\right). \end{aligned} \tag{15}$$

Then we obtain

$$\begin{aligned} \nabla(t) = &\frac{2}{N^2}\sum_{k=1}^{N}\sum_{j=k+1}^{N}\left(\cos\left(\theta_k(t+1) - \theta_j(t+1)\right)\right. \\ &\left. - \cos\left(\theta_k(t) - \theta_j(t)\right)\right) \\ = &\frac{2}{N^2}\sum_{k=1}^{N}\sum_{j=k+1}^{N}\left(\cos\left(\theta_k(t+1) - \theta_j(t+1)\right)\right. \\ &\left. - \cos\left(\theta_k(t+1) - \theta_j(t)\right)\right) + \frac{2}{N^2}\sum_{k=1}^{N}\sum_{j=k+1}^{N} \\ &\left(\cos\left(\theta_k(t+1) - \theta_j(t)\right) - \cos\left(\theta_k(t) - \theta_j(t)\right)\right). \end{aligned} \tag{16}$$

Here, we define

$$\nabla(t) = \nabla_1(t) + \nabla_2(t), \tag{17}$$

where

$$\begin{aligned} \nabla_1(t) = &\frac{2}{N^2}\sum_{k=1}^{N}\sum_{j=k+1}^{N}\left(\cos\left(\theta_k(t+1) - \theta_j(t+1)\right)\right. \\ &\left. - \cos\left(\theta_k(t+1) - \theta_j(t)\right)\right), \\ \nabla_2(t) = &\frac{2}{N^2}\sum_{k=1}^{N}\sum_{j=k+1}^{N}\left(\cos\left(\theta_k(t+1) - \theta_j(t)\right)\right. \\ &\left. - \cos\left(\theta_k(t) - \theta_j(t)\right)\right), \end{aligned}$$

and $\theta_k(t) - \theta_j(t)$ is the two-phase differences between node j and k. When $\nabla_1(t)$ and $\nabla_2(t)$ are positive functions for all time t, $\nabla(t)$ is also positive function.

1. Proof that $\nabla_1(t)$ is positive function for all time t. We have

$$\begin{aligned} \nabla_1(t) = &\frac{2}{N^2}\sum_{k=1}^{N}\sum_{j=k+1}^{N}\left(\cos\left(\theta_k(t+1) - \theta_j(t+1)\right)\right. \\ &\left. - \cos\left(\theta_k(t+1) - \theta_j(t)\right)\right) \end{aligned} \tag{18}$$

$$\begin{aligned} = &\frac{2}{N^2}\sum_{k=1}^{N}\sum_{j=k+1}^{N}\left(\cos\left(\theta_k(t+1) - \theta_j(t+1)\right)\right. \\ &\left. - \cos\left(\theta_k(t+1) - \theta_j(t) + F_j(t)\right)\right). \end{aligned} \tag{19}$$

In this proof we study four cases, and by letting $\phi = \theta_k(t) - \theta_j(t)$ and $\rho = \theta_k(t+1) - \theta_j(t+1)$ we have:

Case 1, $0 \leq \rho \leq \pi$ and $\rho \leq \rho + F_j(t) \leq \pi$,

Case 2, $-\pi \le \rho \le 0$ and $-\pi \le \rho + F_j(t) \le \rho$,
Case 3, $0 \le \phi \le \pi$ and $0 \le \phi + F_k(t) \le \phi$,
Case 4, $-\pi \le \phi \le 0$ and $\phi(t) \le \phi + F_k(t) \le 0$.

$\nabla_1(t)$ is positive for all time t when **Case 1** and **Case 2** are satisfied. Considering **Case 1**, we have

$$0 \le \theta_k(t+1) - \theta_j(t+1) \le \pi, \tag{20}$$
$$\theta_k(t+1) - \theta_j(t+1) \le \theta_k(t+1) - \theta_j(t+1) + F_j(t) \le \pi. \tag{21}$$

From (20) & (21), we derive an inequality condition as

$$\begin{aligned} 0 \;&\le\; F_j(t) \le \pi - \{\theta_k(t+1) - \theta_j(t+1)\} \\ &\Rightarrow 0 \le \sum_{k=1}^{N} K_{jk}(t) \sin\big(\theta_k(t) - \theta_j(t)\big) \le \pi \\ &\quad - \{\theta_k(t+1) \\ &\quad - \theta_j(t+1)\} \\ &\Rightarrow 0 \le \mathbb{E}\Big[\sum_{k=1}^{N} K_{jk}(t) \sin\big(\theta_k(t) - \theta_j(t)\big)\Big] \le \pi \\ &\quad - \mathbb{E}[\theta_k(t+1) - \theta_j(t+1)]. \\ &\quad \text{Then for all } \{\theta_k(t+1) - \theta_j(t+1)\} \in [0, \pi], \\ &\quad \mathbb{E}\big[\theta_k(t+1) - \theta_j(t+1)\big] = \frac{\pi}{2}. \end{aligned} \tag{22}$$

We get

$$0 \le \mathbb{E}\Big[\sum_{k=1}^{N} K_{jk}(t)\Big] \le \frac{\pi}{2}. \tag{23}$$

Considering **Case 2**, we have

$$-\pi \le \theta_k(t+1) - \theta_j(t+1) \le 0, \tag{24}$$
$$-\pi \le \theta_k(t+1) - \theta_j(t+1) + F_j(t) \le \theta_k(t+1) - \theta_j(t+1). \tag{25}$$

From (24) & (25), we derive an inequality condition as

$$\begin{aligned} &-\pi - \{\theta_k(t+1) - \theta_j(t+1)\} \le F_j(t) \le 0 \\ &\Rightarrow -\pi - \{\theta_k(t+1) - \theta_j(t+1)\} \le \sum_{k=1}^{N} K_{jk}(t) \sin\big(\theta_k(t) \\ &\quad - \theta_j(t)\big) \le 0. \\ &\Rightarrow -\pi - \mathbb{E}[\theta_k(t+1) - \theta_j(t+1)] \le \mathbb{E}\Big[\sum_{k=1}^{N} K_{jk}(t) \\ &\quad \sin(\theta_k(t) - \theta_j(t))\Big]. \end{aligned} \tag{26}$$

Then for all $\{\theta_k(t+1) - \theta_j(t+1)\} \in [-\pi, 0]$, we have $\mathbb{E}\big[\theta_k(t+1) - \theta_j(t+1)\big] = -\frac{\pi}{2}$. Then, we get

$$\begin{aligned} -\frac{\pi}{2} &\le -\mathbb{E}\Big[\sum_{k=1}^{N} K_{jk}(t)\Big] \le 0 \\ &\Rightarrow 0 \le \mathbb{E}\Big[\sum_{k=1}^{N} K_{jk}(t)\Big] \le \frac{\pi}{2}. \end{aligned} \tag{27}$$

2. Proof that $\nabla_2(t)$ is positive function for all time t. We have

$$\begin{aligned} \nabla_2(t) &= \frac{2}{N^2} \sum_{k=1}^{N} \sum_{j=k+1}^{N} \big(\cos\big(\theta_k(t+1) - \theta_j(t)\big) \\ &\quad - \cos\big(\theta_k(t) - \theta_j(t)\big)\big) \\ &= \frac{2}{N^2} \sum_{k=1}^{N} \sum_{j=k+1}^{N} \big(\cos\big(\theta_k(t) - \theta_j(t) + F_k(t)\big) \\ &\quad - \cos\big(\theta_k(t) - \theta_j(t)\big)\big). \end{aligned} \tag{28}$$

$\nabla_2(t)$ is positive for all time t when the **Case 3** and **Case 4** are satisfied. Considering **Case 3**, we have

$$0 \le \theta_k(t) - \theta_j(t) \le \pi, \tag{29}$$
$$0 \le \theta_k(t) - \theta_j(t) + F_k(t) \le \theta_k(t) - \theta_j(t). \tag{30}$$

From (29) & (30), we derive the inequality condition as

$$\begin{aligned} 0 \;&\le\; \theta_k(t) - \theta_j(t) + F_k(t) \le \theta_k(t) - \theta_j(t) \\ &\Rightarrow -\{\theta_k(t) - \theta_j(t)\} \le F_k(t) \le 0 \\ &\Rightarrow -\{\theta_k(t) - \theta_j(t)\} \le \sum_{k=1}^{N} K_{kj}(t) \sin\big(\theta_j(t) - \theta_k(t)\big) \le 0 \\ &\Rightarrow 0 \le \sum_{j=1}^{N} K_{kj}(t) \sin\big(\theta_k(t) - \theta_j(t)\big) \le \{\theta_k(t) - \theta_j(t)\}. \end{aligned}$$

For all $\{\theta_k(t) - \theta_j(t)\} \in [0, \pi]$, we have

$$\mathbb{E}\big[\theta_k(t) - \theta_j(t)\big] = \frac{\pi}{2}.$$

We get

$$\begin{aligned} 0 \;&\le\; \mathbb{E}\Big[\sum_{j=1}^{N} K_{kj}(t) \sin\big(\theta_k(t) - \theta_j(t)\big)\Big] \le \mathbb{E}\big[\theta_k(t) - \theta_j(t)\big] \\ &\Rightarrow 0 \le \mathbb{E}\Big[\sum_{j}^{N} K_{kj}(t)\Big] \le \frac{\pi}{2}. \end{aligned} \tag{31}$$

Considering **Case 4**, we have

$$-\pi \le \theta_k(t) - \theta_j(t) \le 0 \tag{32}$$
$$\theta_k(t) - \theta_j(t) \le \theta_k(t) - \theta_j(t) + F_k(t) \le 0. \tag{33}$$

From (32) & (33), we derive the inequality condition as

$$\begin{aligned} &\theta_k(t) - \theta_j(t) \le \theta_k(t) - \theta_j(t) + F_k(t) \le 0 \\ &\Rightarrow 0 \le F_k(t) \le -\{\theta_k(t) - \theta_j(t)\} \\ &\Rightarrow 0 \le \sum_{j=1}^{N} \sin\big(\theta_j(t) - \theta_k(t)\big) \le -\{\theta_k(t) - \theta_j(t)\} \\ &\Rightarrow 0 \le -\sum_{j=1}^{N} K_{kj}(t) \sin\big(\theta_k(t) - \theta_j(t)\big) \le -\{\theta_k(t)\theta_j(t)\}. \end{aligned} \tag{34}$$

For all $\{\theta_k(t) - \theta_j(t)\} \in [-\pi, 0]$, then $\mathbb{E}\big[\theta_k(t) - \theta_j(t)\big] = -\frac{\pi}{2}$.

We get

$$0 \leq -\mathbb{E}\left[\sum_{j=1}^{N} K_{kj}(t)\sin\left(\theta_k(t)-\theta_j(t)\right)\right] \leq \mathbb{E}\left[\theta_k(t)-\theta_j(t)\right]$$

$$\Rightarrow 0 \leq \mathbb{E}\left[\sum_{j=1}^{N} K_{kj}(t)\right] \leq \frac{\pi}{2}. \tag{35}$$

From (23), (27), (31) & (35), $\nabla(t) \geq 0$ when the summation of the coupling strength satisfies with condition as

$$0 \leq \mathbb{E}\left[\sum_{j=1}^{N} K_{kj}(t)\right] \leq \frac{\pi}{2}. \tag{36}$$

From (3), we have

$$0 \leq \alpha\mathbb{E}\left[\sum_{j=1}^{N} K_{kj}(t-1)\right] + \beta\mathbb{E}\left[\sum_{k=1}^{N} |\sin\left(\theta_k(t-1)-\theta_j(t-1)\right|)\right] \leq \frac{\pi}{2}.$$

$$\Rightarrow \leq \alpha\mathbb{E}\left[\sum_{j=1}^{N} K_{kj}(t)\right] + \beta N \leq \frac{\pi}{2}. \tag{37}$$

Therefore, to guarantee that the condition in (37) is always true, each element of the coupling strength K_{kj} must initialize with uniform random in the interval $\left[0, \frac{\pi}{2N}\right]$, and the phase oscillator $\theta_i(t) \in [0, \pi]$. As noticed in (23), (27), (31), and (35), $\nabla_1(t)$ and $\nabla_2(t)$ are positive for all time, where α lies in the range of $[-1, 1]$, and $\beta = \frac{\pi(1-\alpha)}{4N}$. According to (16), $\nabla(t)$ is also positive within the range of α and β, so the updated function of Lyapunov candidate $\nabla(t+1)$ is always greater than $\nabla(t)$ for all time. Hence, the Lyapunov candidate $\nabla(t)$ will converge to one at time t. In addition, the vector elements of phase centroid will converge to one according to (13), which ends the proof. □

V. PERFORMANCE EVALUATION

In this section, we evaluate the performance of the proposed algorithm under various network environments. In this simulation, we generate six WBANs, where each one can occupy one sensor node. The sensor node is uniformly distributed within each seat. The detail of the types of sensor used in this simulation can be found in Table 1 We consider a hospital waiting room for the simulation scenario. We choose the network size as $20m \times 20m$, which is shown in Fig. 4. In the simulation, the control parameter for the utility with $b = 1$ and $c = 9$ as in Fig. 2 are used. The details of the simulation parameters are given in Table 2 [13].

For the path loss model, we adopt the IEEE P802.15 channel model for body area network [20], which is given by

$$G_{ii} = 6.6\log_{10} d + 36.1 + N_0 \tag{38}$$

where d is the distance between transmitter and receiver.

As shown in Fig. 5, the utility values of all sensor nodes converge to the same value, indicating the QoS of each user is fairly adjusted among the neighboring WBANs. U_1, U_2, U_3, and U_4 are the utility values of the sensor type 3, 2, 1, 4 as shown in Table 2, and U_5 and U_6 are the utility values of the sensor type 3 and 2 respectively. It is clear in Fig. 6, that the power of all sensors reach convergence at around iteration 15. This implies that the transmission powers are adjusted so that only the required power is consumed by sensor nodes to reach the required data rate. In Fig. 7, the data rate D_1, D_2, D_3, and D_4 converge to the highest possible value of the required data rate, according to the utility values. while the data rate D_5 and D_6 coincide with D_1 and D_2, respectively, because they are the same types of sensor. Since the utility value converged to approximately 0.9 (utility value ranges from 0 to 1), the achieved data rate cannot be as high as the required value in the Table 2.

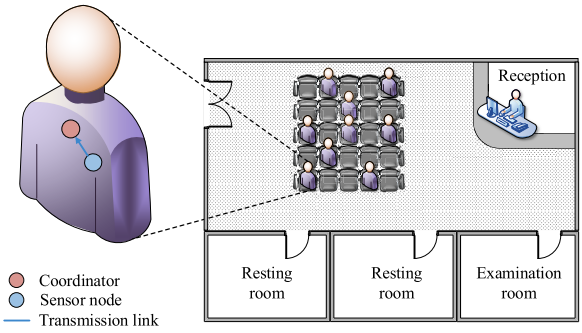

FIGURE 4. WBANs within hospital environment.

TABLE 2. Simulation parameters.

Parameter	Value
Utility shape	$a = 1, b = 9$
Network size	20m × 20m
Number of seat	5 to 30
Distance between each seat	1m
Location of sensor nodes	Uniformly distributed on seat
Location of coordinator	Center of the seat
Seat size	0.25m radius
Initial transmission power	Uniformly random between (-20,5) dBm
Bandwidth	1MHz
Noise (N_0)	-32 dBm
Convergence error (ϵ)	10^{-4}

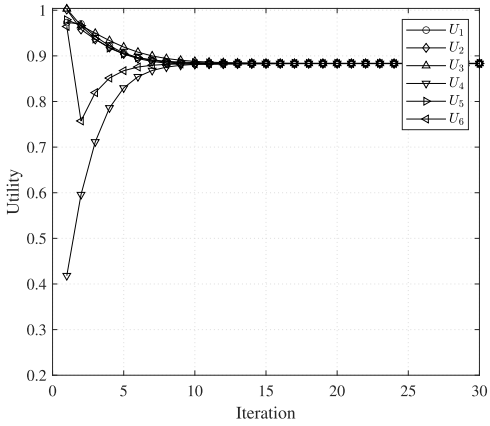

FIGURE 5. Utility values of the proposed algorithm.

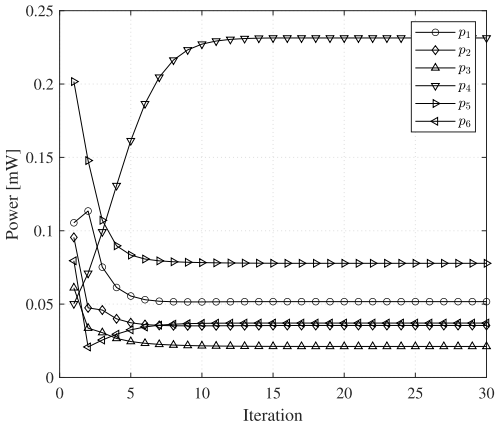

FIGURE 6. Transmit power of the proposed algorithm.

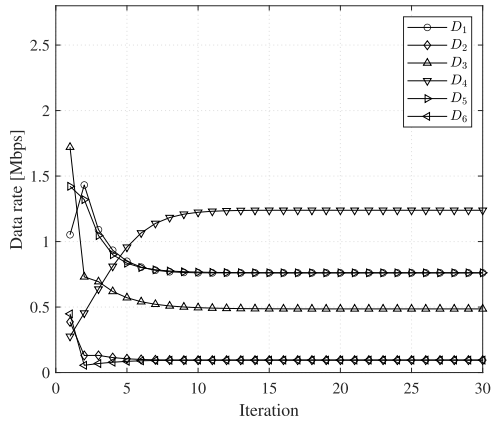

FIGURE 7. Data rate of the proposed algorithm.

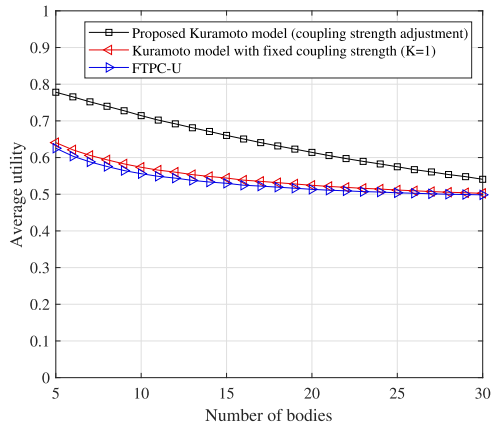

FIGURE 8. Average utility values of the proposed algorithm, FTPC-U, and Kuramoto with constant coupling strength.

We compare the performance of the proposed algorithm with Kuramoto model with constant coupling strength and Flocking-based transmission power control with utility (FTPC-U) [25] using the same environment for fair comparison. In the Kuramoto model with *constant* coupling strength, we set the coupling strength for the model to $K = 1$. Overall, according to Figs. 8, 9, 10, it is noticeable that the proposed algorithm performs significantly better than the Kuramoto model with constant coupling strength and FTPC-U. In Fig. 8,

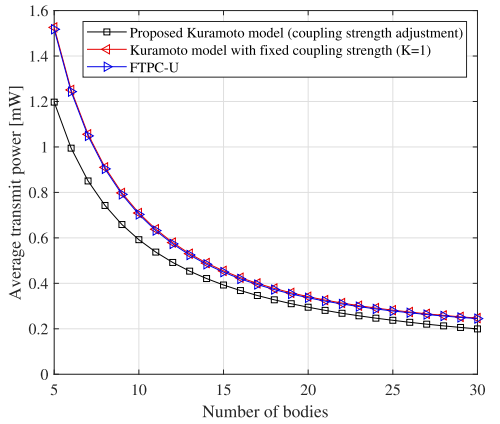

FIGURE 9. Average transmit power of the proposed algorithm, FTPC-U, and Kuramoto with constant coupling strength.

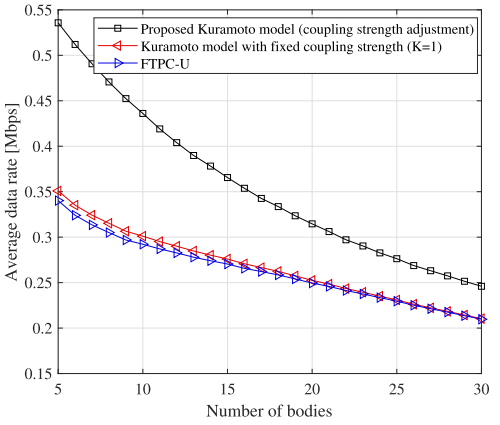

FIGURE 10. Average data rate of the proposed algorithm, FTPC-U, and Kuramoto with constant coupling strength.

the result shows that the average the QoS of each user under the proposed algorithm is around 20 percent higher than those of the Kuramoto model with constant coupling strength and FTPC-U. The average utility value of the proposed algorithm drops slightly as the number of node grows, but it still outmatches the Kuramoto model with constant coupling strength and FTPC-U. Additionally, the proposed algorithm uses less power as in Fig. 9, while obtaining around 0.2 Mbps more data rate than the Kuramoto model with constant coupling strength and FTPC-U, as shown in Fig. 10. According to Fig. 10, after the number of WBAN increases to about 20, the proposed algorithm still acquires approximately 0.1 Mbps more data rate in average than both the comparison algorithms.

In the following figure, we compare the convergence performance of the proposed algorithm with the Kuramoto model with *constant* coupling strength and FTPC-U. As illustrated by Fig. 11, the number of rounds required for the proposed to reach convergence is below ten while the Kuramoto model and FTPC-U need more rounds to achieve convergence. The significant difference between the convergence speed of the proposed and the Kuramoto is due to the coupling strength coefficient adjustment $K_{ij}(t)$ as mentioned in (3) was applied to the proposed algorithm. As the number of bodies

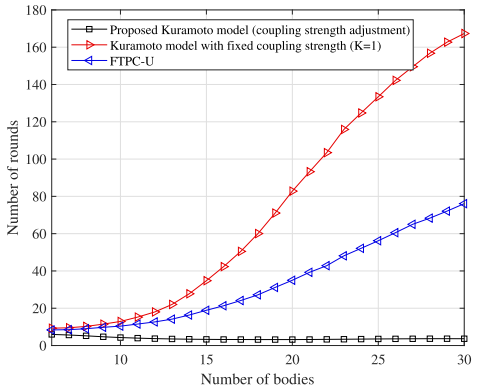

FIGURE 11. The average number of rounds required to reach a stable equilibrium under the proposed algorithm, FTPC-U, and Kuramoto with constant coupling strength.

increases, FTPC-U needs about eighty number of rounds, and the Kuramoto model needs nearly twice as that of the FTPC-U to obtain convergence, whereas the proposed requires approximately the same number of rounds to acquire convergence through out the number of bodies in the network.

VI. CONCLUSION

In this paper, a transmission power control scheme based on Kuramoto model was introduced for WBAN environment, which provides QoS fairness and improved power efficiency for users. In addition to the original Kuramoto model, we use the Kuramoto model with coupling strength coefficient adjustment to enhance the synchronization speed. Moreover, we prove the range of convergence for the Kuramoto model. The proposed method works with different types of sensor within each WBANs. We use a utility function to regulate and indicate the QoS of each user. The transmit power is controlled in relation to the utility value, providing that the utility values are synchronized. The simulation results demonstrate that the transmission power control algorithm is QoS-effective, power efficient, and sufficient for mitigating inter-network interference in dense network environment.

In the future, we plan to carry out experiment regarding the proposed algorithm on actual WBAN hardware test-bed within practical environment which involves participants of various age groups, sex, and medical applications. In addition, we have a plan to expand the proposed algorithm suitable for multi-hop environments, the key feature of which would be avoiding hidden node problem.

REFERENCES

[1] W. Zang, S. Zhang, and Y. Li, "An accelerometer-assisted transmission power control solution for energy-efficient communications in WBAN," *IEEE J. Sel. Areas Commun.*, vol. 34, no. 12, pp. 3427–3437, Dec. 2016.

[2] M. Roy, C. Chowdhury, and N. Aslam, "Designing an energy efficient WBAN routing protocol," in *Proc. 9th Int. Conf. Commun. Syst. Netw. (COMSNETS)*, Bengaluru, India, Jan. 2017, pp. 298–305.

[3] P. K. D. Pramanik, A. Solanki, A. Debnath, A. Nayyar, S. El-Sappagh, and K. S. Kwak, "Advancing modern healthcare with nanotechnology, nanobiosensors, and Internet of nano things: Taxonomies, applications, architecture, and challenges," *IEEE Access*, vol. 8, pp. 65230–65266, 2020.

[4] P. K. D. Pramanik, A. Nayyar, and G. Pareek, "WBAN: Driving e-healthcare beyond telemedicine to remote health monitoring: Architecture and protocols," in *Telemedicine Technologies*. New York, NY, USA: Academic, 2019, pp. 89–119.

[5] A. Kurian and R. Divya, "A survey on energy efficient routing protocols in wireless body area networks (WBAN)," in *Proc. Int. Conf. Innov. Inf., Embedded Commun. Syst. (ICIIECS)*, Coimbatore, India, Mar. 2017, pp. 1–6.

[6] B. Johny and A. Anpalagan, "Body area sensor networks: Requirements, operations, and challenges," *IEEE Potentials*, vol. 33, no. 2, pp. 21–25, Mar. 2014.

[7] P. K. D. Pramanik, G. Pareek, and A. Nayyar, "Security and privacy in remote healthcare: Issues, solutions, and standards," in *Telemedicine Technologies*. New York, NY, USA: Academic, 2019, pp. 201–225.

[8] B. Mahapatra, R. Krishnamurthi, and A. Nayyar, "Healthcare models and algorithms for privacy and security in healthcare records," in *Security and Privacy of Electronic Healthcare Records: Concepts, Paradigms and Solutions*. London, U.K.: IET, 2019, p. 183.

[9] D. Fernandes, A. G. Ferreira, R. Abrishambaf, J. Mendes, and J. Cabral, "A low traffic overhead transmission power control for wireless body area networks," *IEEE Sensors J.*, vol. 18, no. 3, pp. 1301–1313, Feb. 2018.

[10] Y. Xu, M. Ke, F. Liu, and Q. Zha, "A self-adaptive power control algorithm based on game theory for inter-WBAN interference mitigation," in *Proc. 2nd IEEE Int. Conf. Comput. Commun. (ICCC)*, Chengdu, China, Oct. 2016, pp. 2873–2877.

[11] S. Boccaletti, J. Kurths, G. Osipov, D. Valladares, and C. Zhou, "The synchronization of chaotic systems," *Phys. Rep.*, vol. 366, nos. 1–2, pp. 1–101, 2002.

[12] J.-Y. Jung, H.-H. Choi, and J.-R. Lee, "Survey of bio-inspired resource allocation algorithms and MAC protocol design based on a bio-inspired algorithm for mobile ad hoc networks," *IEEE Commun. Mag.*, vol. 56, no. 1, pp. 119–127, Jan. 2018.

[13] D. D. Olatinwo, A. Abu-Mahfouz, and G. Hancke, 2019, "A survey on LPWAN technologies in WBAN for remote health-care monitoring," *Sensors*, vol. 19, no. 23, p. 5268, 2019.

[14] Y. Kuramoto, "Self-entrainment of a population of coupled non-linear oscillators," in *Proc. Int. Symp. Math. Problems Theor. Phys.*, in Lecture Notes in Physics. Berlin, Germany: Springer, 1975, pp. 420–422.

[15] L. Scardovi, "Clustering and synchronization in phase models with state dependent coupling," in *Proc. 49th IEEE Conf. Decis. Control (CDC)*, Atlanta, GA, USA, Dec. 2010, pp. 627–632, doi: 10.1109/CDC.2010.5718119.

[16] O. Simeone, U. Spagnolini, Y. Bar-Ness, and S. Strogatz, "Distributed synchronization in wireless networks," *IEEE Signal Process. Mag.*, vol. 25, no. 5, pp. 81–97, Sep. 2008, doi: 10.1109/MSP.2008.926661.

[17] C. Kirst, M. Timme, and D. Battaglia, "Dynamic information routing in complex networks," *Nature Commun.*, vol. 7, no. 1, pp. 1–9, Apr. 2016.

[18] A. Papachristodoulou and A. Jadbabaie, "Synchonization in oscillator networks with heterogeneous delays, switching topologies and nonlinear dynamics," in *Proc. 45th IEEE Conf. Decis. Control*, San Diego, CA, USA, Dec. 2006, pp. 4307–4312, doi: 10.1109/CDC.2006.376762.

[19] R. C. Moioli, P. A. Vargas, and P. Husbands, "Exploring the kuramoto model of coupled oscillators in minimally cognitive evolutionary robotics tasks," in *Proc. IEEE Congr. Evol. Comput.*, Barcelona, Spain, Jul. 2010, pp. 1–8, doi: 10.1109/CEC.2010.5586486.

[20] (2012). *I. WG802.15*. [Online]. Available: http://ieee802.org/15/

[21] W.-B. Yang and K. Sayrafian-Pour, "Interference mitigation for body area networks," in *Proc. IEEE 22nd Int. Symp. Pers., Indoor Mobile Radio Commun.*, Toronto, ON, Canada, Sep. 2011, pp. 2193–2197, doi: 10.1109/PIMRC.2011.6139905.

[22] J. A. Acebrón, L. L. Bonilla, C. J. P. Vicente, F. Ritort, and R. Spigler, "The Kuramoto model: A simple paradigm for synchronization phenomena," *Rev. Mod. Phys.*, vol. 77, no. 1, p. 137, Apr. 2005.

[23] K. Suzuki, H. Nishiyama, N. Kato, H. Ujikawa, K.-I. Suzuki, and N. Yoshimoto, "A bandwidth allocation method to improve user QoS satisfaction without decreasing system throughput in wireless access networks," in *Proc. IEEE 23rd Int. Symp. Pers., Indoor Mobile Radio Commun. (PIMRC)*, Sydney, NSW, Australia, Sep. 2012, pp. 1430–1435.

[24] W.-H. Kuo and W. Liao, "Utility-based radio resource allocation for QoS traffic in wireless networks," *IEEE Trans. Wireless Commun.*, vol. 7, no. 7, pp. 2714–2722, Jul. 2008.

[25] C. Lee and J. Lee, "QoS-based interference mitigation scheme in wireless body area networks," in *Proc. Int. Conf. Inf. Commun. Technol. Converg. (ICTC)*, Jeju, South Korea, Oct. 2017, pp. 610–615.

KIMCHHEANG CHHEA received the B.S. degree from the Department of Electrical and Energy Engineering, Institute of Technology of Cambodia, Phnom Penh, Cambodia, in 2019. He is currently pursuing the M.S. and Ph.D. degrees integrated program with the School of Electrical and Electronics Engineering, Chung-Ang University, Seoul, South Korea. His current research interests include bio-inspired algorithms, wireless body area networks, and machine learning-based 5G communication systems.

DARA RON received the B.S. degree from the Department of Electrical and Energy Engineering, Institute of Technology of Cambodia (ITC), Phnom Penh, Cambodia, in 2017. He is currently pursuing the integrated M.S. and Ph.D. degrees with the School of Electrical and Electronics Engineering, Chung-Ang University, South Korea. His current research interests include bio-inspired algorithms, LoRaWAN protocol, and artificial intelligent-based wireless networks.

JUNG-RYUN LEE (Senior Member, IEEE) received the B.S. and M.S. degrees in mathematics from Seoul National University, in 1995 and 1997, respectively, and the Ph.D. degree in electrical and electronics engineering from the Korea Advanced Institute of Science and Technology (KAIST), in 2006. From 1997 to 2005, he was a Chief Research Engineer with LG Electronics, South Korea. From 2006 to 2007, he was a full time Lecturer of electronic engineering with the University of Incheon. Since 2008, he has been a Professor with the School of Electrical and Electronics Engineering, Chung-Ang University, South Korea. His research interests include low energy networks and algorithms, bio-inspired autonomous networks, and artificial intelligence-based networks. He is a member of IEICE, KIISE, and KICS.